Passive Sensing Using Multiple Types of Communication Signal Waveforms for Internet-of-Everything

Junlin Zhang, Zeming Li, Yunfei Chen, *Senior Member, IEEE*, Weidang Lu, *Senior Member, IEEE*, Fei Yi, and Mingqian Liu, *Member, IEEE*

***Abstract*—Passive sensing using communication signal waveforms is considered to be a promising technology for target monitoring in Internet-of-Everything. Conventional passive sensing schemes require accurate estimation of the time difference of arrival (TDOA) and frequency difference of arrival (FDOA), which is leading to high complexity but low accuracy. In this paper, a robust passive sensing algorithm using multiple illumination of opportunities is proposed to improve the detection performance while avoiding separate estimation of TDOA and FDOA. The proposed method first combines the linear constrained minimum variance adaptive filter with the wide nulling algorithm to achieve target direction finding while separating the direct wave and suppressing multipath interference. Then, the Linear Canonical Transformation-based Cross Ambiguity Function (LCTCAF) is employed to estimate the distance and radial velocity of the target. Relying on the relationship between distance to time and velocity to Doppler, a Distance-Velocity transformation-based Cross Ambiguity Function (DVCAF) is introduced to characterize the distance and radial velocity of the target. Finally, a spectral peak search scheme is exploited in DVCAF to estimate the time delay and Doppler shift so as to identify the target parameters directly. Its' Cramer-Rao Low Bound is derived. Simulation results validate that the performance of the proposed algorithm outperforms the conventional estimators based on the cross ambiguity function.**

***Index Terms*—Communication signal waveforms, cross ambiguity function (CAF), Internet-of-Everything, parameter estimation, passive target sensing.**

I. Introduction

With the continuous innovation of information and communication technologies, the Internet of Things (IoT) is affecting the many aspects of social life space [1], [2]. Internet-of-Everything (IoE) has become an essential aspect of wireless networks [3]. The proliferation of IoE applications has resulted in an exponential rise in the number of intelligent devices and intelligent systems [4]–[6]. Radar system is a typical intelligent system, which can efficiently sense and track valuable targets in the monitored area and thus has an attractive application perspective in IoT, such as smart cities, smart homes, smart manufacturing, smart transportation. Passive target sensing, or passive bistatic radar, is an important setting of radar [7]. In particular, performing target sensing using communication signal waveforms is a promising paradigm, which allows target sensing and communication to share common hardware modules and signal processing modules, and improve the spectrum efficiency by utilizing the same waveform for both purposes.

The passive sensing paradigm directly exploits various existing communication signal waveforms in the ambient radio environment to detect the interested target, providing numerous advantages such as strong low-altitude detection capability, effective anti-stealth potential, robust anti-jamming capability, and flexible installation and deployment options. With the rapid development of radio and television broadcasting, mobile communication, navigation communication and satellite technology, the available illuminators of opportunities continue to expand, including FM broadcasting, Digital Audio Broadcasting (DAB), Digital Video Broadcasting-Terrestrial (DVB-T), China Mobile Multimedia Broadcasting (CMMB), Wi-Fi and many other types [8], [9]. The diverse range of illuminators possess distinctive benefits in regard to coverage range, resolution capabilities, and application environments, which promotes the advancement of the passive radar paradigm in the field of target detection.

In the passive radar paradigm, the estimation of parameters related to the position and velocity of the target from the echo signals is essential to achieve target detection and localization. The parameters include Direction of Arrival (DOA), Time Difference of Arrival (TDOA), and Frequency Difference of Arrival (FDOA). A number of effective methods have been developed in the literature. In [10], Qu *et al*. proposed a localization algorithm based on iterative constrained weighted least squares, which have high estimation accuracy and less computation results. In order to address the system errors in passive positioning systems, FDOA and TDOA were used to improve the situation according to [11], [12]. In [13], [14], Code Division Multiple Access (CDMA) signals were applied

This work was supported by the National Natural Science Foundation of China under Grant 62301380, 62231027 and 62071364, in part by the Natural Science Basic Research Program of Shaanxi under Grant 2024JC-JCQN-63, in part by the China Postdoctoral Science Foundation under Grant 2022M722504, in part by the Postdoctoral Science Foundation of Shaanxi Province under Grant 2023BSHEDZZ169, in part by the Key Research and Development Program of Shaanxi under Grant 2023-YBGY-249, in part by the Guangxi Key Research and Development Program under Grant 2022AB46002 and in part by the Fundamental Research Funds for the Central Universities under Grant XJSJ23090. *(Corresponding author: Weidang Lu.)*

J. Zhang, Z. Li, F. Yi, M. Liu are with the State Key Laboratory of Integrated Service Networks, Xidian University, Shaanxi, Xi'an 710071, China, (e-mail: zhangjunlin@xidian.edu.cn; stezmli@stu.xidian.edu.cn; yysysnsohu@qq.com; mqliu@mail.xidian.edu.cn).

Y. Chen is with Department of Engineering, University of Durham, Durham, UK DH1 3LE (e-mail: Yunfei.Chen@durham.ac.uk).

W. Lu is with the College of Information Engineering, Zhejiang University of Technology, Hangzhou 310023, China (e-mail: luweid@zjut.edu.cn).

for the passive positioning systems to enhance the flexibility and effectiveness of passive positioning, as well as its anti-jamming performance. In [15], Liu *et al*. proposed an external illumination positioning algorithm based on FDOA and applied it to a single satellite positioning system. The results proved that this algorithm has high estimation accuracy and faster convergence speed compared to traditional algorithms. In [16] and [17], FDOA was combined with TDOA and the application scenarios are extended to dual-satellite systems. In [18], Shamaei *et al*. utilized the received cellular Long Term Evolution (LTE) signals to jointly extract the TOA and DOA. This framework introduced three tracking loops to refine the estimates. In [19], Gogineni *et al*. used Universal Mobile Telecommunications System (UMTS) signals as external illuminators in multi-base radar systems, corrected the estimation errors of time delay and Doppler shift, and provided the error-corrected Cramer-Rao Lower Bound (CRLB). In [20], a novel passive target detection scheme was presented based on a real-life cooperative 5G network. This scheme employed a 5G signal as external illuminator of opportunity. In [21], Sendall *et al*. utilized FM frequency modulation broadcast as an external illuminator and proposed a target localization technique based on time delay and Doppler shift, and the proposed method has been proven to be more accurate than distance-only or Doppler-only techniques. In [22], Shi *et al*. utilized FM commercial radio signals to compute the joint CRLB of the target parameter estimation error. A direct target positioning method different from traditional two-step estimation methods is proposed in [23], which characterize the target's position and speed-related parameters in the signal, and directly estimate the position and speed of the target through iterative search. In [24]–[26], the Kalman filter was introduced and improved in passive positioning systems, and the target's position were solved through recursive filtering and adaptive filtering methods. In [27], Yu *et al*. applied the virtual time reversal method to passive localization and achieved rapid passive localization. However, many existing algorithms are designed using only one type of illuminator, failing to make the most of the multiple types available illuminators in the electromagnetic spectrum. As a result, the estimation accuracy of the existing methods is unsatisfactory, compromising the reliability of the positioning.

To improve the target sensing performance, this paper first proposes a Linear Canonical Transformation-based Cross Ambiguity Function (LCTCAF) based on the traditional method, and then combines the idea of Direct Positioning Determination (DPD) to propose a Distance-Velocity transformation-based Cross Ambiguity Function (DVCAF) method. DVCAF characterizes the time delay and frequency shift in terms of distance and velocity based on the relationship between the distance and time delay, velocity and frequency shift, and substitutes them into the echo signal equation, in order to realize the direct estimation of distance and velocity. Since the estimated distances from different illuminators are similar, they can be fused to improve the estimation accuracy. Compared with the traditional method, the proposed method only performs one estimation operation and has a strong noise suppression capability. Thus, this method can theoretically improve the detection accuracy. The main motivations and contributions of this paper are summarized as follows.

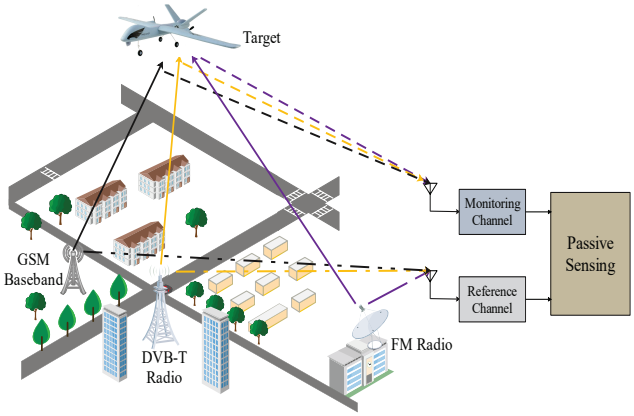

Fig. 1. Framework of passive sensing system based on multiple illuminators.

- We develop a target detection algorithm based on TDOA and FDOA, which exploits multiple non-cooperative electromagnetic signals to detect targets, including FM radio, DVB-T radio, and GSM communication base stations.
- To accommodate low Signal-to-Noise Ratio (SNR) scenarios, LCTCAF is introduced to estimate time delay and Doppler shift associated with the distance and radial velocity of the flight target accurately.
- The DVCAF method is proposed to directly estimate the distance and velocity of the target, which avoids the time overhead and error accumulation caused by step-by-step estimation.
- We derive the CRLB for the proposed DVCAF and the LCTCAF in this scenario and verify the effectiveness of the proposed methods through simulation experiments.

The remainder of this paper is organized as follows. In Section II, we present the system model and the signal model. In Section III, we detailly discuss the estimation of distance and radial velocity based on LCTCAF. In Section IV, we analyze the estimation of distance and radial velocity based on DVCAF. In Section V, we talk about the estimation of the velocity of the moving target. In Section VI, we discuss the CRLB for the estimation of localization parameters of the moving target. Simulation experiment results are presented and analyzed in Section VII. Moreover, the conclusion of the paper is in Section VIII.

II. SYSTEM MODEL

A. System model

The considered system is illustrated in Fig. 1. This system consists of three external illuminators (DVB-T radio, FM radio, and GSM) and a receiving station. The receiving station has two channels: monitoring channel and reference channel. The communication waveforms from external illuminators are illuminated on the target, and the reflected echo signals are received by the receiving station. The monitoring channel receives the target echo waveforms, while the reference channel receives the direct waveforms from the external illuminator.

Since the orientation of external illuminators is known, we only concentrate on the monitoring channel.

B. signal model

Considering the presence of multiple direct waves in the reference channel, it is necessary to first separate the different direct waves before obtaining pure direct wave signals. The operating frequencies of these heterogeneous illuminators are different. Thus, a filter can be used to separate them. In this case, the direct signal waveform of the ith illuminator $x_i(t)$ can be expressed as

$$x_i(t) = b_i s_i(t) + n_i(t), \tag{1}$$

where b_i denotes the amplitude of the ith direct wave signal, $s_i(t)$ denotes the direct wave signal of the ith illuminator (DVB-T radio, FM radio, GSM), and $n_i(t)$ denotes the ith additive zero-mean Gaussian noise.

The echo signal $y(t)$ in the monitoring channel can be expressed as

$$\begin{aligned} y(t) = &\sum_{i=1}^{M} a_i s_i(t-\tau_i) e^{-j2\pi f_{di} t} + \sum_{i=1}^{M} d_i s_i(t) \\ &+ \sum_{i=1}^{M}\sum_{j=1}^{N} m_{ij} s_i(t-\tau_{ij}) + n(t), \end{aligned} \tag{2}$$

where $s_i(t-\tau_i)$ is the echo signal of different illuminators, τ_i is the time delay of the echo signal of the ith illuminator relative to the direct wave signal, f_{di} is the Doppler shift of the echo signal corresponding to the direct wave, a_i denotes the amplitude of the echo signal of the ith illuminator; d_i is the amplitude of different direct wave signals in the reference channel, $\sum_{i=1}^{M}\sum_{j=1}^{N} m_i s_i(t-\tau_{ij})$ denotes the multipath signal component in the echo signal, H is the number of path of the multipath channel, m_{ij} is the amplitude of the jth path signal of the direct wave signal of the ith illuminator, τ_{ij} is the time delay of the jth path signal of the ith illuminator relative to the direct wave.

Because the illumination signal is not for detection, the echo signal in the monitoring channel is usually weak. Its' power is much lower than that of direct wave interference and multipath interference. In order to extract the echo signal in the monitoring channel, we need to suppress the direct wave interference and multipath interference. In the scenario of low SNR, spatial filtering is used, among which the adaptive method is a highly effective spatial filtering method [28]. To deal with direct wave interference, the Linearly Constrained Minimum Variance (LCMV) algorithm can be used to constrain the direction of the direct wave emitted by the external illuminators [29]. To deal with multipath interference, it is necessary to use a wide-nulling method to produce nulling in the direction of multipath interference for suppression [30]. After the suppression of the two kinds of interference, we can obtain a better echo signal as

$$y(t) = \sum_{i=1}^{M} a_i s_i(t-\tau_i) e^{-j2\pi f_{di} t} + n(t). \tag{3}$$

III. Joint distance and radial velocity estimation based on LCTCAF

A. Linear Canonical Transformation-based Cross Ambiguity Function

Because the propagation path of the echo signal is different from the direct wave signal, there will be a time delay relative to the direct wave signal. At the same time, because of the relative velocity between the target and the transmitting station, the echo signal will also have a frequency offset, that is, Doppler shift. In order to improve the estimation accuracy in the low SNR environment, we first transform the signal and then construct a linear canonical transformation-based cross ambiguity function to process the echo signal and direct wave signal. The linear canonical transformation of $f(t)$ can be expressed as [31]

$$\begin{aligned} &F_{(a,b,c,d)}(u) = L_{(a,b,c,d)}(f(t)) \\ &= \begin{cases} \sqrt{\frac{1}{j2\pi b}} e^{j(\frac{d}{2b}u^2 - \frac{1}{b}ut + \frac{a}{2b}t^2)} f(t)dt & b \neq 0, \\ \sqrt{d} e^{j\frac{cd}{2}u^2} f(du) & b = 0, \end{cases} \end{aligned} \tag{4}$$

where the parameters a, b, c and d satisfy $ad - bc = 1$, and the signal is transformed from the time domain to u domain, which is not physically defined by a linear canonical transformation.

The cross ambiguity function (CAF) is a two-dimensional function of time delay and Doppler shift, which enables the detection of signals based on the correlation between the signals, and the localization situations can be obtained based on the spectral peak search at the same time. The LCTCAF $A_{L_{(a,b,c,d)}}(u, w)$ can be obtained for the linear canonical transformed signal, but it is worth noting that in the LCTCAF, u and w only have mathematical meaning but not physical meaning. However, passive detection estimates the velocity of the target position by estimating the time delay and the Doppler shift. Therefore, u and w alone can not directly determine the estimated values of delay and Doppler. It is necessary to find out the corresponding relationship between u, w, and time delay τ, and Doppler shift f.

By decomposing the free parameter matrix, we can obtain [31]

$$\begin{bmatrix} a & b \\ c & d \end{bmatrix} = \begin{bmatrix} 1 & 0 \\ \frac{d-1}{b} & 1 \end{bmatrix} \cdot \begin{bmatrix} 1 & b \\ 0 & 1 \end{bmatrix} \cdot \begin{bmatrix} 1 & 0 \\ \frac{a-1}{b} & 1 \end{bmatrix}. \tag{5}$$

According to the superposition of linear canonical transformation, we can obtain

$$\begin{aligned} &L_{(a,b,c,d)}(f(t)) \\ &= L_{(1,0,\frac{d-1}{b},1)}(L_{(1,b,0,1)}(L_{(1,0,\frac{a-1}{b},1)}(f(t)))). \end{aligned} \tag{6}$$

This is equivalent to applying of linear canonical transformation three times to $f(t)$.

According to the product property and the convolution property of the linear canonical transformation and the cross ambiguity function [31], we can infer the corresponding relationship of the LCTCAF and CAF, as

$$A_{L(a,b,c,d)}(\tau, v) = A_f(d\tau - bv, -c\tau + av). \tag{7}$$

It can be seen that the LCTCAF of the signal can be regarded as the translation and expansion of the CAF of the signal,

and the value of ambiguity function spectrum is a one-to-one correspondence. This indicates that LCTCAF can still be used to estimate the echo parameters of moving targets. Note that the horizontal and vertical coordinate axes of the spectrum of LCTCAF are not the time domain parameters and the frequency domain parameters but a mathematically defined domain with no actual physical meaning, which is essentially the stretching transformation and Doppler shift of CAF. By transforming the parameters of (7), the relationship between LCTCAF and CAF can be expressed as

$$A_{L(a,b,c,d)}(u,w) = A_f(du - bw, -cu + aw). \tag{8}$$

Therefore, relying on the spectral peak search of the result processed by LCTCAF, the searched optimal values of u and w can be transformed into the estimated value of time delay τ and Doppler shift f, using

$$\tau = du - bw, \tag{9}$$

$$f = -cu + aw. \tag{10}$$

The specific steps of the spectral peak search are summarized in Algorithm 1.

Algorithm 1 The spectral peak search

1: Initialize parameters and obtain the result of Cross Ambiguity Function;
2: Store the data of the two-dimensional section of the Cross Ambiguity Function into the array W', where the ith element is denoted as w_i;
3: Make a backward difference on the elements in the array W' and deposit the result into the array W'', the jth element of the array is denoted as w_j'', and $w_j'' = w_i' - w_{i+1}'$.
4: Set the elements less than zero in W'' to zero, count the number of elements of the array w'' that is greater than zero and record them as n, and then transform the n elements as $\eta = \frac{1}{n}\sum_{j=1}^{n} W_j{}''$, $w_j'' = w_j'' - \frac{(\eta)^2}{w_j''}$.
5: Repeat the operation of Step 3 until $n = 1$, and output the following table of the elements greater than zero as the result of the spectral peak search.

B. Distance and radial velocity estimation

In the application scenario targeted by this method, the geometric relationship between the target, the illuminator, and the receiving station is shown in Fig. 2, and it satisfies the following realtionship

$$\begin{cases} R_t + R_r = L + c\tau \\ R_t^2 = R_r^2 + L^2 - 2R_r L\cos\theta_R, \end{cases} \tag{11}$$

where θ_R denotes the angle between the line of the illuminator and the target and the line of the receiving antenna and the target, L denotes the distance between the receiving station and the illuminator, R_t denotes the distance between the target and the illuminator, and R_r denotes the distance between the target and the receiving station.

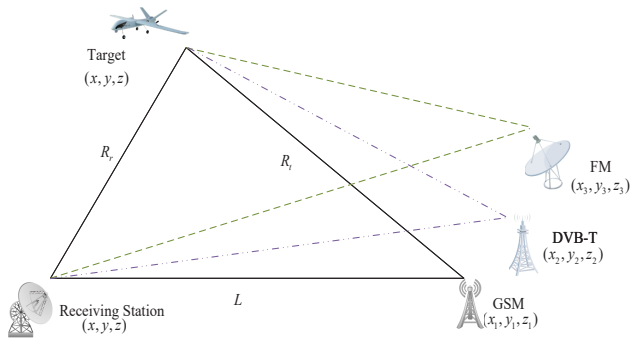

Fig. 2. The geometric relationship diagram between the target, illuminator, and receiving station.

It can be obtained by the transformation that

$$R_r = \frac{c^2\tau^2 + 2c\tau}{2(L + c\tau - l\cos\theta_R)}. \tag{12}$$

The radial velocity v_d and the Doppler shift f satisfy

$$v_d = \lambda f_d, \tag{13}$$

where λ denotes the wavelength of the illumination signal.

According to (12) and (13), the time delay estimate v and the Doppler shift estimate f can be converted into the distance estimate R and the radial velocity estimate v. Because the position and signal wavelength of different illuminators are different, the estimated u_{max}, w_{max} of different illuminators are different from each other, and the estimated values of time delay v_i and Doppler shift f_{di} are also different, the subscript i denotes the ith radiation source. However, after converting v_i, f_{di} into the distance and radial velocity estimates, the distance estimation R_i of different illuminators are theoretically the same.

The distance estimation R_i of different illuminators can be weighted fused by a weighted fusion method that minimizes the sum of Mean Square Error (MSE). The weight corresponding to the estimated result R_i of the ith illuminator is

$$w_i^* = \frac{1}{P_i \widetilde{P}}, \tag{14}$$

$$P_i = \mathbb{E}[(\overline{R} - \tilde{R}_i)^2], \tag{15}$$

$$\widetilde{P} = \sum_{k=1}^{M'} \frac{1}{P_k}, \tag{16}$$

where $\mathbb{E}\{\cdot\}$ denotes mathematical expectation, $\overline{R}$ denotes the average value of the estimated distance of different illuminators.

In conclusion, the main procedure of the LCTCAF algorithm is summarized in Algorithm 2.

IV. Joint distance and radial velocity estimation based on the DVCAF

A. Distance-Velocity transformation-based Cross Ambiguity Function

In Section III, we proposed a target localization algorithm based on LCTCAF. Through (8), we can find the relationship

Algorithm 2 The LCTCAF algorithm

1: Separate direct wave signals by bandpass filters;
2: Suppress the direct wave interference and multipath interference in the echo channel by LCMV adaptive filtering algorithm and wide nulling algorithm. And obtain the two-dimensional DOA information of echo signal by frequency scanning;
3: Process different direct waves and echoes by LCTCAF, and obtain the peak value of three-dimensional spectrum by spectral peak search, then obtain the optimal value of u and w;
4: Convert the optimal value of u and w to the estimated value of time delay v and the estimated value of frequency shift f_{di} according to (9) and (10);
5: Convert the estimated value of time delay v and the estimated value of frequency shift f_{di} to the estimated value of distance R_i and the estimated value of radial velocity V_{di} according to (12) and (13) ;
6: Fuse the estimated value of distance R_i of different illuminators according to (14) ;

between LCTCAF and CAF so that we can convert LCTCAF to CAF by scaling. The CAF of the direct wave signal and echo signal of an illuminator is

$$\begin{aligned}\chi_i(\tau,f) &= \int_{-\infty}^{\infty} x_t^*(t)x_i(t+\tau)e^{j2\pi ft}dt \\ &= \int_{-\infty}^{\infty} x_t^*(t)b_i s_i(t+\tau)e^{j2\pi ft}dt,\end{aligned} \tag{17}$$

where τ and f are the time delay and the Doppler shift of the direct wave signal. To simplify it, we have

$$\begin{aligned}&\chi_i(\tau,f) \\ &= \int_{-\infty}^{\infty}(\sum_{i=1}^{M} a_i s_i^*(t-\tau_i)e^{j2\pi f_{di}t+v(t)}b_i s_i(t+\tau)e^{-j2\pi ft}dt \\ &= \int_{-\infty}^{\infty} a_i b_i s_i^*(t+\tau_i)s_i(t+\tau)e^{-j2\pi(f-f_{di})t}dt,\end{aligned} \tag{18}$$

Due to the same process for each illuminator, we can deduce a kind of illuminator first, and (18) can be simplified as

$$\chi_i(\tau,f) = \int_{-\infty}^{\infty} s^*(t+\tau_i)s(t+\tau)e^{-j2\pi(f-f_{di})t}dt. \tag{19}$$

When τ=τ_i and $f = f_d$, $\chi_i(\tau,f)$ takes the maximum value, so the CAF can be constructed to estimate the time delay and the Doppler shift of echo signals from different illuminators by changing the time delay and the Doppler shift of the direct wave signals, and then combine the results of two-dimensional DOA estimation to obtain the position and the radial velocity of the target respectively. Finally, the location results of different illuminators are fused with the fusion algorithm so as to realize the localization of the target.

However, this method is a two-step method, which requires estimating the time delay and Doppler parameters first and then making a fusion estimation after transforming the time delay and Doppler estimation results into the estimation of the position and velocity of the target. Each estimation process is accompanied by a certain accuracy loss. In order to reduce the accuracy loss of the estimation, we propose the DVCAF in this paper.

By transforming (12) and (13), it can be obtained that

$$\tau = \frac{\sqrt{L^2+R_r^2-2R_rL\cos\theta_R}+R_r-L}{c}, \tag{20}$$

$$f = \frac{v_d}{\lambda}, \tag{21}$$

where λ denotes the wavelength of the signal of the illuminator.

By substituting both the mapping functions of time delay to distance and the mapping function of Doppler shift to radial velocity into the equation of CAF, it can be obtained that

$$\begin{aligned}\chi(\tau,f) = &\int_{-\infty}^{\infty} s^*(t+\frac{\sqrt{L^2+R_r^2-2R_rL\cos\theta_R}+R_r-L}{c}) \\ &s(t+\tau)e^{j2\pi(f-\frac{v_d}{\lambda})}dt,\end{aligned} \tag{22}$$

Since L and λ are all known and θ_R has been estimated by the method proposed in Section III, we no longer need to search for τ and f. Instead, we can directly search for the distance from the target to the receiving station R_t and the radial velocity v_d of the target.

$$\begin{aligned}\chi(R,v) = &\int_{-\infty}^{\infty} s^*(t+\frac{\sqrt{L^2+R_r^2-2R_rL\cos\theta_R}+R_r-L}{c}) \\ &s(t+\frac{\sqrt{L^2+R^2-2RL\cos\theta_R}+R-L}{c})e^{j2\pi(\frac{v}{\lambda}-\frac{v_d}{\lambda})}dt.\end{aligned} \tag{23}$$

In (23), R_r denotes the real distance to be estimated, and v_d denotes the radial velocity of the target to be estimated. Obviously, when $R = R_r$ and $v = v_d$, the objective function $\chi(R,v)$ obtains the maximum value.

B. Feature level fusion of multiple types illuminators

In this part, we propose a new estimation method. After the transformation in (20) and (21), the estimation results of different illuminators are unified. That is, the distance estimation results of different illumination signals are all the same in theory. Thus, different direct waves and echo signals can be directly processed by the DVCAF, and then the sum of different DVCAF can be obtained as

$$\chi(R,v_1\cdots v_i) = \sum_{i=0}^{M}\chi^{(i)}(R,v_i), \tag{24}$$

where $\chi^{(i)}(R,v_i)$ denotes the DVCAF of the ith illuminator and the echo signal. It is worth mentioning that the expected estimate of distance is the same for all illuminators. However, the expected estimate of radial velocity is not the same, so there may be multiple peaks in the velocity dimension, and the correct result may not be obtained for the illuminator CAF with velocity sub-peaks. Therefore, the idea of this method is only to use the hybrid ambiguity function to obtain its distance estimation, then substitute it into the respective DVCAF function to get its velocity section, and then search its peak value as the radial velocity estimation value.

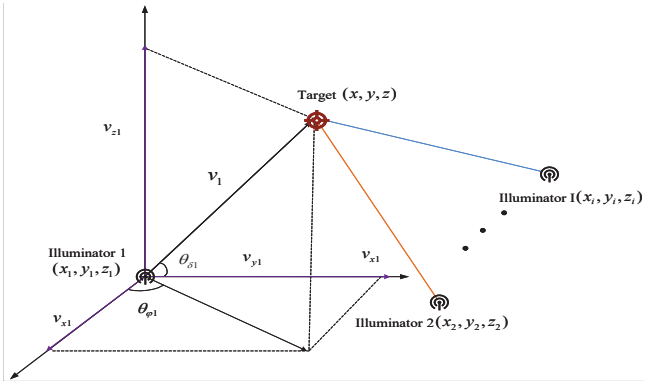

Fig. 3. The velocity decomposition diagram of the target in 3D space.

In conclusion, the main procedure of estimating distance and radial velocity by DVCAF are summarized in Algorithm 3.

Algorithm 3 Estimating distance and radial velocity by DVCAF algorithm

1: Separate direct wave signals by bandpass filters;
2: Suppress the direct wave interference and multipath interference in the echo channel by LCMV adaptive filtering algorithm and wide nulling algorithm. And obtain the two-dimensional DOA information of the echo signal by frequency scanning;
3: Use the DVCAF shown in (23) to process different direct waves and echoes, then superimpose the obtained three-dimensional maps;
4: Obtain the peak of the hybrid DVCAF function by spectral peak research and obtain the estimated value of the distance $\hat{R}$;
5: Intercept the two-dimensional section of $R = \hat{R}$ in the DVCAF function of each illuminator, and search for the peak to determine the estimated radial velocity $\hat{v}_{di}$;

V. Velocity Estimation of the Moving Target

After the distance between the target and the receiving station R_r and the radial velocity of the target v_{di} are obtained by spectral peak search, the position of the target in the three-dimensional space can be solved as

$$\begin{cases} R_r &= \sqrt{(x-x_i)^2+(y-y_i)^2+(z-z_i)^2} \\ R_t &= \sqrt{(x-x_s)^2+(y-y_s)^2+(z-z_s)^2} \\ L &= \sqrt{(x_s-x_i)^2+(y_s-y_i)^2+(z_s-z_i)^2}, \end{cases} \tag{25}$$

where (x, y, z), (x_1, y_1, z_1), (x_i, y_i, z_i) denotes the coordinates of the target, the receiving station and the ith illuminator in the three-dimensional space respectively. The position parameters of the receiving station and the illuminator are known, so that the values of R_r, R_t, L are available. Thus, the position (x, y, z) of the target in the three-dimensional space can be obtained.

As shown in Fig.4, since the coordinates of the target in the three-dimensional space can be solved by (25), the azimuth angle θ_{φ_i} and the pitch angle θ_{δ_i} of the ith illuminator relative to the target can be calculated from the coordinated of the target and the illuminator. θ_{φ_1} denotes the azimuth angle of the illuminator 1 relative to the target, θ_{δ_1} denotes the pitch angle of the illuminator 1 relative to the target. The velocity component of the target velocity in the direction of the connection between the target and the ith external illuminator is the estimated radial velocity $v_i = v_{di}$, the relative velocity v_1 between the illuminator 1 and the target can be decomposed into v_{x1},v_{y1},v_{z1} in the Cartesian three-dimensional space coordinate system, and the solution equation can be expressed as

$$\begin{cases} v_{x1} &= v_1 \cos\theta_{\delta_1} \cos\theta_{\varphi_1} \\ v_{y1} &= v_1 \cos\theta_{\delta_1} \sin\theta_{\varphi_1} \\ v_{z1} &= v_1 \sin\theta_{\delta_1}, \end{cases} \tag{26}$$

Similarly, we can calculate the velocity component v_{xi}, v_{yi}, v_{zi} of the relative v_i between the illuminator i and the target. When the number of external illuminators $i \geq 3$, and the connection of different illuminators to the target is not in the same plane, the velocity v of the target can be synthesized by the radial velocity v_i corresponding to different illuminators, which can be expressed as

$$v_x = \sum_{i=1}^{I} v_{xi}, \tag{27}$$

$$v_y = \sum_{i=1}^{I} v_{yi}, \tag{28}$$

$$v_z = \sum_{i=1}^{I} y_{zi}, \tag{29}$$

$$v = \sqrt{v_x^2 + v_y^2 + v_z^2}. \tag{30}$$

VI. CRLB of Localization Parameters Estimation

Assuming that the echo channel signal $y(t)$ contains only the echo signal and noise after pre-processing. Thus, $y(t)$ is as [32], [33]

$$y(t) = \sum_{i=1}^{M} a_i s_i(t-\tau_i) e^{-j2\pi f_{di} t} + n(t). \tag{31}$$

For the ith echo in the echo signal, its energy can be expressed as

$$\mathcal{E}_i = \int_{-\infty}^{\infty} a_i^2 |s_i(t-\tau_i)|^2 dt. \tag{32}$$

The autocorrelation function of the noise can be expressed as

$$\mathbb{E}\{n(t)n^*(t')\} = N_0 \delta(t-t'), \tag{33}$$

where $\delta\{\cdot\}$ denotes Dirac-delta function, $(\cdot)^*$denotes complex conjugate, t' denotes a fixed value.

In the previous sections, we have derived the relationship between distance and delay as

$$\tau_i = \frac{R_{ti} + R - L_i}{c} = g(R), \tag{34}$$

$$f_{di} = \frac{v_{di}}{\lambda} = h(v_{di}). \tag{35}$$

Substitute (34) and (35) into (31), we can obtain that

$$y(t) = \sum_{i=1}^{M} a_i s_i(t - g(R)) e^{-j2\pi v_{di} t} + n(t). \tag{36}$$

It can be seen that the vector to be estimated is mainly composed of distance R and radial velocity v_{di}, which can be expressed as

$$\theta = [R, v_{d1}, v_{d2}, v_{d3}, L, v_{dM}]. \tag{37}$$

The probability density function of the echo signal $y(t)$ can be expressed as (38) on the top of this page. Then the algorithm of the probability density function can be expressed as

$$\begin{aligned} &\ln p(y;\theta) = K \ln K \\ &- \frac{K}{N_0} \int_{-\infty}^{\infty} |y(t) - \sum_{i=1}^{M} a_i s_i(t - g(R)) e^{-j2\pi h(v_{di})t}|^2 dt. \end{aligned} \tag{39}$$

The derivative of (39) with respect to the distance R and the radial velocity v_{di} can be expressed as

$$\begin{aligned} &\frac{\partial \ln p(y;\theta)}{\partial R} = -\frac{2}{N_0} \\ &\times \mathrm{Re} \int_{-\infty}^{\infty} n^*(t) \sum_{i=1}^{M} a_i s_i(t - g(R)) g'(R) e^{-j2\pi h(v_{di})t} dt, \end{aligned} \tag{40}$$

$$\begin{aligned} &\frac{\partial \ln p(y;\theta)}{\partial v_{di}} = -\frac{4\pi}{N_0} \\ &\times \mathrm{Im} \int_{-\infty}^{\infty} a_i t n^*(t) s_i(t - g(R)) e^{-j2\pi h(v_{di})t} h'(v_{di}) dt, \end{aligned} \tag{41}$$

where $s_i(t) = ds_i(t)/dt$, $\mathrm{Re}\{g\}$ denotes real part and $\mathrm{Im}\{g\}$ denotes imaginary part.

When estimating unknown parameters, the CRLB of unbiased estimation should satisfy

$$\mathrm{V}(\hat{\theta}_i)_{\mathrm{CRLB}} \geq [I^{-1}(\theta)]_{i,j}, \tag{42}$$

where $[I^{-1}(\theta)]_{i,j}$ denotes the element of the i th row and j th column of the Fisher Information Matrix (FIM), the element of the m th row and n th column of the FIM can be expressed as

$$[I(\theta)]_{i,j} = I_{j,i} = \mathbb{E}\left\{ \frac{\partial \ln p(y;\theta)}{\partial \theta_i} \frac{\partial \ln p(y;\theta)}{\partial \theta_j} \right\}. \tag{43}$$

To simplify the derivation, we present Lemma 1 as follows.

Lemma 1: If we use Ψ to represent SNR, and define the following variables

$$\Psi_i = \frac{\mathcal{E}_i}{N_0}, \tag{44}$$

$$G_i = \frac{1}{\mathcal{E}_i} \int_{-\infty}^{\infty} a_i^2 t^2 |s_i(t)|^2 dt, \tag{45}$$

$$L_i = \frac{1}{\mathcal{E}_i} \int_{-\infty}^{\infty} a_i^2 |s_i(t)|^2 dt, \tag{46}$$

$$Q_i = \frac{1}{\mathcal{E}_i} Im \int_{-\infty}^{\infty} a_i^2 t s_i(t) s_i^*(t) dt, \tag{47}$$

$$H_i = \frac{1}{\mathcal{E}_i} Im \int_{-\infty}^{\infty} s_i(t) s_i^*(t) dt, \tag{48}$$

$$P_i = \frac{1}{\mathcal{E}_i} \int_{-\infty}^{\infty} a_i^2 |s_i(t)|^2 dt. \tag{49}$$

Then, one has

$$A_i = L_i, \tag{50}$$

$$B_i = (Q_i + g(R) H_i), \tag{51}$$

$$C_i = (G_i + 2P_I g(R) - g(R)^2 \mathcal{E}_i), \tag{52}$$

Thus, one has

$$\mathrm{V}(\hat{R})_{\mathrm{CRLB}} = \frac{c^2}{2\Psi} \frac{1}{\sum\limits_{i=1}^{M} \frac{A_i C_i - B_i^2}{C_i}}, \tag{53}$$

$$\mathrm{V}(\hat{v}_{di})_{\mathrm{CRLB}} = \frac{c^2}{2\Psi} \frac{A_i + \sum\limits_{m=1(m\neq i)}^{M} \frac{A_m C_m - B_m^2}{C_m}}{C_i \sum\limits_{m=1}^{M} \frac{A_m C_m - B_m^2}{C_m}}. \tag{54}$$

The proof of Lemma 1 is shown in Appendix A.

The CRLB of the LCTCAF is the same as the traditional two-step estimation method, and its CRLB can be expressed as [34]

$$\mathrm{V}(\widetilde{\tau}_i)_{\mathrm{CRLB}} = \frac{1}{2\Psi} \cdot \frac{C_i}{A_i C_i - B_i^2}, \tag{55}$$

$$\mathrm{V}(\widetilde{f}_{di})_{\mathrm{CRLB}} = \frac{1}{8\pi^2 \Psi} \cdot \frac{A_i}{A_i C_i - B_i^2}. \tag{56}$$

Note that R_t and L are all constants and have no effect on the estimation accuracy of velocity and distance, while R and f_{di} are variables to be estimated, which will affect the estimation accuracy of distance and radial velocity. Therefore, the CRLB of distance and velocity of LCTCAF can be derived from the representation of the CRLB of the non-random parameter functions as follows

$$\begin{aligned} \mathrm{V}(\widetilde{R}_i)_{\mathrm{CRLB}} &= c^2 \mathrm{V}(\widetilde{\tau}_i)_{\mathrm{CRLB}} \\ &= \frac{c^2}{2\Psi} \cdot \frac{C_i}{A_i C_i - B_i^2}, \end{aligned} \tag{57}$$

$$\begin{aligned} \mathrm{V}(\widetilde{v}_{di})_{\mathrm{CRLB}} &= {\lambda_i}^2 \mathrm{V}(\widetilde{f}_{di})_{\mathrm{CRLB}} \\ &= \frac{{\lambda_i}^2}{8\pi^2 \Psi} \cdot \frac{A_i}{A_i C_i - B_i^2}. \end{aligned} \tag{58}$$

It is worth explaining that the traditional method first converts the time delay and Doppler parameters into the distance and radial velocity parameters, then synthesizes the three-dimensional velocity of the target with different radial velocities. Therefore, the CRLB of radial velocity can be used for velocity estimation, and by transforming (54), it can be obtained that

$$\begin{aligned} \mathrm{V}(\hat{v}_{di})_{\mathrm{CRLB}} &= \frac{{\lambda_i}^2}{8\pi^2 \Psi} \frac{A_i + \sum\limits_{m=1(m\neq i)}^{M} \frac{A_m C_m - B_m^2}{C_m}}{C_i \sum\limits_{m=1}^{M} \frac{A_m C_m - B_m^2}{C_m}} \\ &\leq \frac{{\lambda_i}^2}{8\pi^2 \Psi} \frac{A_i}{A_i C_i - B_i^2} \\ &= \mathrm{V}(\widetilde{v}_{di})_{\mathrm{CRLB}}. \end{aligned} \tag{59}$$

$$p(y;\theta) = K\exp\{\ln K\} + K\exp\{-\frac{1}{N_0}\cdot\int_{-\infty}^{\infty}|y(t)-\sum_{i=1}^{M}a_i s_i(t-g(R))e^{-j2\pi h(v_{di})t}|^2 dt\}. \tag{38}$$

It can be seen from the above formula that the CRLBs of the two estimation methods are equivalent when and only when the number of illuminators $M = 1$. If $M > 1$, the proposed DVCAF has a lower velocity CRLB. This is because the different radial velocity v_{di} of the traditional method can not be fused when there are fewer illuminators, but the DVCAF method improves the accuracy of v_{di} while fusing R. When there are enough illuminators, the traditional method can also use the data fusion algorithm to fuse the radial velocity, and the velocity CRLBs of both methods are the same.

In the traditional method, M distance values are estimated from different illuminators, and then different distance estimates are fused according to (8) to (10). Finally, the CRLB of distance estimation can be expressed as

$$\begin{aligned} \mathrm{V}(\widetilde{R})_{\mathrm{CRLB}} &= \frac{c^2}{2\Psi}\frac{1}{\sum_{i=1}^{m}\frac{A_i C_i - B_i^2}{C_i}} \\ &= \mathrm{V}(\hat{R})_{\mathrm{CRLB}}. \end{aligned} \tag{60}$$

VII. Simulation Results and Discussion

In this section, we evaluate the performance of the proposed method by simulation. We select the DVB-T signal, FM signal, and GSM signal as the test signals. The power ratio of the three direct wave signals is 1: 0.08: 0.0025 , and the carrier frequencies are 750MHz, 97MHz, and 955MHz, respectively. The echo signal is 40dB weaker than that of the direct wave signal, and the number of coherent cumulative points of the signal is 10^6. The noise is additive white Gaussian. The target distance is 10km, and the sub-velocity in the three directions of the illuminator is 200 m/s. The SNR is set as the SNR of the echo signal to the noise, and 500 Monte-Carlo trials are carried out for each SNR. The Normalized Minimum Mean Squared Error (NMSE) is used as the evaluation criterion of the proposed method, which is defined as

$$\mathrm{NMSE} = \frac{|\hat{y} - y|^2}{y^2}, \tag{61}$$

where y is the expected output, $\hat{y}$ is the estimated value. Correspondingly, in order to match the NMSE and to better show the estimation performance in the same coordinates, we normalize the CRLB to obtain the Normalized CRLB (NCRLB), which is expressed as

$$\mathrm{V}(\hat{\phi})_{\mathrm{NCRLB}} = \frac{\mathrm{V}(\hat{\phi})_{\mathrm{CRLB}}}{\phi^2}, \tag{62}$$

where $\mathrm{V}(\hat{\phi})_{\mathrm{CRLB}}$ is the value of CRLB, ϕ is the theoretical value of parameter estimation.

For SNR from -50dB to 10dB, we combine CAF, LCTCAF, and DVCAF with different external illuminators, and construct the scenarios as follows:

- DVB-T: DVB-T–CAF, DVB-T–LCTCAF, DVB-T–DVCAF;
- GSM: GSM–CAF, GSM–LCTCAF, GSM–DVCAF;
- FM: FM–CAF, FM–LCTCAF, FM–DVCAF.

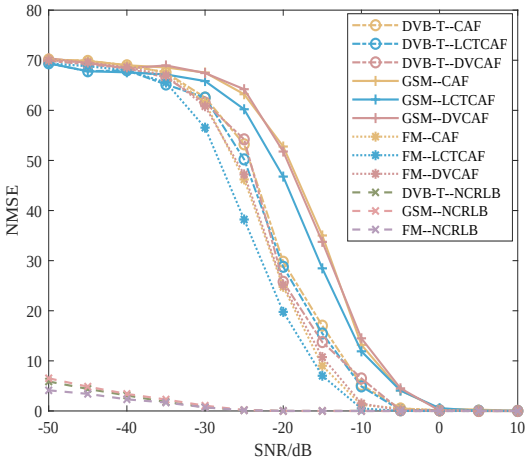

Fig. 4. The distance estimation performance with SNR for different illuminators.

To serve as a control, we also give the NCRLB of the three illuminators, which are DVB-T–NCRLB, GSM–NCRLB and FM–NCRLB.

Fig. 4 illustrates the target distance estimation performance for different illuminators, demonstrating that the estimation performance of CAF, LCTCAF, and DVCAF methods all improve with the increase of SNR. When using different signals as external illuminators (FM signal, DVB-T signal and GSM signal), the estimation accuracy of the three methods reaches 10^{-3} at -10dB, -5dB, and 0dB, respectively. However, the distance estimation performance of the three methods for the same illuminator is relatively close. This is because, in the scenario of the same single external illuminator, the three methods are not significantly different, especially the DVCAF estimation method is substantially the same as CAF.

Fig. 5 illustrates the target distance estimation performance in the scenario of multiple types of external illuminators, demonstrating that the estimation performance of CAF, LCTCAF, and DVCAF methods all improve with the increase of SNR and gradually approaching NCRLB. From Fig. 5, it can be seen that the estimation accuracy of the three methods reaches 10^{-3} at -10dB. For low SNR, the estimation performance of DVCAF is better than that of CAF and LCTCAF. This is because both CAF and LCTCAF estimate the time delay first without the noise suppression. When the SNR is low, the high-power noise has a large impact on the time delay estimation. Even though the information fusion method is subsequently used to fuse the distance estimation results of different illuminators, the accuracy improvement is limited. However, DVCAF can directly mix and fuse the ambiguity function when estimating the distance, the distance estimates can be accumulated, but the noise background of

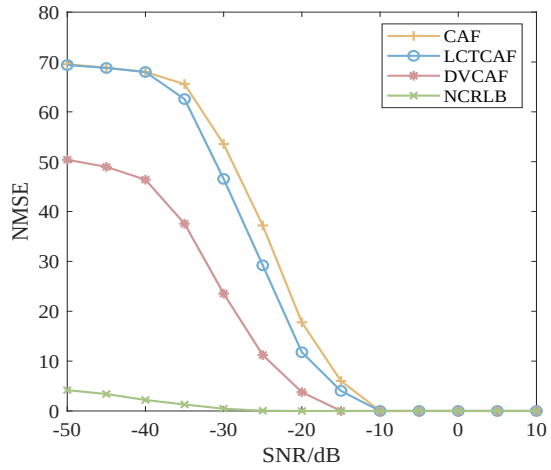

Fig. 5. The distance estimation performance with SNR.

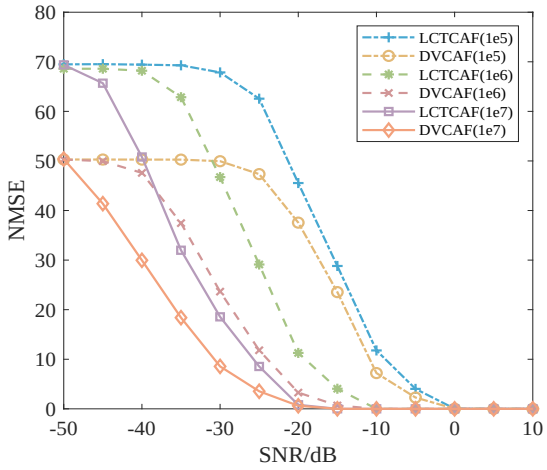

Fig. 7. The distance estimation performance with coherent cumulative points.

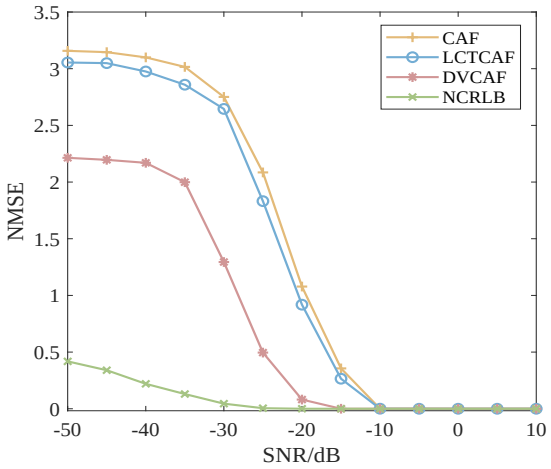

Fig. 6. The velocity estimation performance for different methods with SNR.

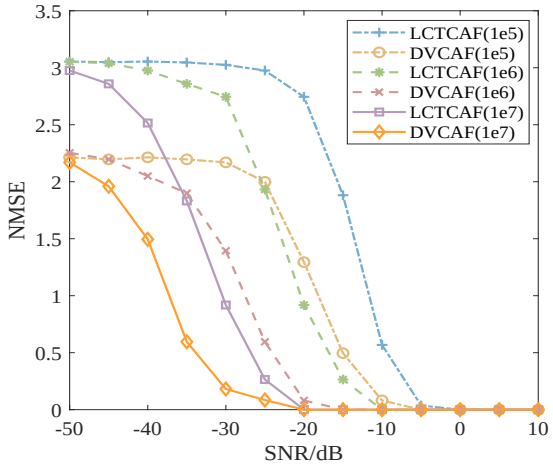

Fig. 8. The velocity estimation performance with coherent cumulative points.

different CAFs is different from each other, and when the fusion is performed, the noise will not accumulate but will cancel each other out. Thus, DVCAF has a good effect of noise suppression. In addition, compared with Fig. 4, the estimation performance of the proposed method is better than that of the single external illuminator in the scenario of multiple external illuminators. The computational complexity of one search of LCTCAF is $O((P+1)(2(M+1)+(M+1)/2\log_2(2M+1)))+P(MN\log_2 MN+MN\log_2 M))$, where M is the number of sampling points, P is the number of external illuminators, and N is the number of cycles in the frequency domain. And the computational complexity of one search of DVCAF is $O(PMN\log_2 MN+MN\log_2 M)$. Due to the absence of linear canonical transformation and the smaller amount of data processed by the spectral peak search, the computational complexity of DVCAF is lower than that of LCTCAF.

Fig. 6 illustrates the target velocity estimation performance in the scenario of multiple types of external illuminators, demonstrating that CAF, LCTCAF, and DVCAF can all estimate the target velocity by using multiple types of external illuminators. With the increase of the SNR, the estimation performance is continuously improved. However, as shown in Fig. 6, DVCAF can achieve an estimation accuracy of 10^{-3} at -15dB, but CAF and LCTCAF can only achieve this estimation accuracy at -10dB. This is because different radial velocities can not be fused when using CAF and LCTCAF, but the results of DVCAF benefit from the operation of fusion, therefore, DVCAF has higher estimation accuracy and stronger noise suppression than the other two methods.

Under the condition of different coherent cumulative point numbers of 10^5, 10^6 and 10^7 respectively, we conduct the simulation experiments using LCTCAF and DVCAF in the scenario of multiple types of external illuminators.

As seen in Fig. 7, the performance of the distance estimation with different coherent cumulative points is gradually improved with the increase of SNR. When the SNR is the same, the more coherent the cumulative points, the higher the estimation performance, this is because the echo gain will increase as the number of coherent cumulative points increases, and the noise suppression effect will also be stronger.

As seen in Fig. 8, the accuracy of the velocity estimation of LCTCAF and DVCAF is gradually improved with the increase

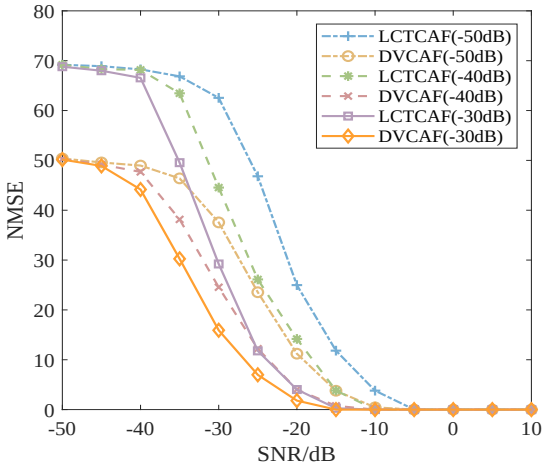

Fig. 9. The distance estimation performance for SDR with SNR.

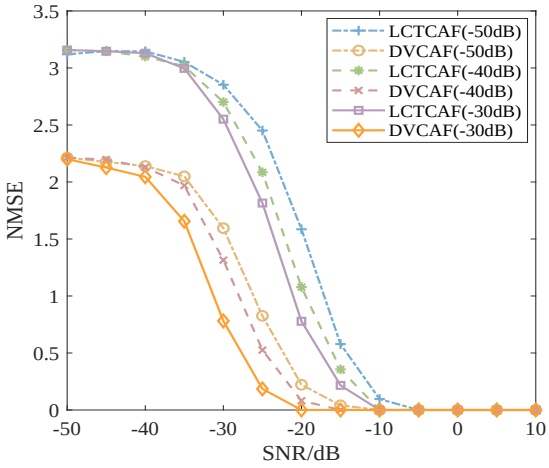

Fig. 10. The velocity estimation performance for SNR with SDR.

of coherent cumulative points. When the number of the point is 10^7, the NMSE of DVCAF at -20dB is already less than 10^3. Thus, increasing the number of coherent cumulative points can also improve the velocity estimation accuracy of LCTCAF and DVCAF.

The power ratio between echo and direct wave, which is called Signal-to-Direct wave Ratio (SDR), is an important parameter, and the estimation performance with different SDR can be used to evaluate the detection ability of position and velocity estimation algorithms for stealthy targets. For SDRs of -50dB, -40dB, and -30dB, we conduct the simulation experiments and make comparisons through the results.

As shown in Fig. 9, when the SNR is fixed, the distance estimation performance of DVCAF and LCTCAF improves continuously with the decrease of SDR. When SDR is -50dB, the estimation accuracy of the DVCAF algorithm has achieved 10^{-3} when the SNR is -15dB, this is because the SNR is the power ratio between echo signal and noise, when the SNR is fixed, the decrease of SDR means the enhancement of the direct wave power, and the spectral peak characteristics of DVCAF and LCTCAF will be more obvious due to the enhancement of the direct wave power. Therefore, the results of the spectral peak search will be less affected by the noise, and the estimation accuracy will be higher.

As shown in Fig. 10, when the SNR is fixed,the estimation accuracy of the target velocity is inversely proportional to the value of SDR. When SDR is -50dB, the estimation accuracy of DVCAF has achieved 10^{-3} when the SNR is -20dB, which shows that increasing SDR can effectively improve the velocity estimation accuracy.

VIII. Conclusions

This paper has developed a novel target detection algorithm based on TDOA and FDOA by employing multi-irradiation sources, which fully utilizes the advantages of CAF and linear canonical transformation. The proposed method avoids stepwise estimation of the target parameters, thus decreasing time overhead and enhancing parameter estimation precision. The results of the simulation has indicated that the proposed algorithm provides significantly higher accuracy in estimating target distance and velocity than the conventional LCTCAF and CAF. Furthermore, it can be observed from the results that the proposed scheme can provide large performance gains by improving the SNR of the echo signal to the noise, the Signal-to-Direct wave Ratio (SDR) and the number of coherent cumulative points under low to medium SNR conditions. Although the proposed method effectively tackles the error accumulation caused by step-by-step estimation, it cannot avoid the estimation error introduced by the linear regular ambiguity function estimator. In future work, we will aim to develop a convenient and reliable passive sensing scheme using multiple external Illuminators to achieve high-accuracy detecting of small-low-mantle targets.

Appendix A
Proof of Lemma 1

According to the variables and mapping relationships from (44) to (52), each element of the FIM can be calculated by these equations, and the results of the elements are shown from (63) to (65) on the top of the next page, and I_{other} can be given by

$$I_{other} = \frac{\partial^2 \ln p(y;\theta)}{\partial v_{dj} \partial v_{di}} = 0, \tag{66}$$

where $i, j = 1, 2, \cdots, L, M$, $i \neq j$ and $g'(R) = dg(R)/dR$, $h'(v_{di}) = dh(v_{di})/dv_{di}$ which can be calculated according to (34) and (35) as follows

$$g'(R) = dg(R)/dR = \frac{1}{c}, \tag{67}$$

$$h'(v_{di}) = dh(v_{di})/dv_{di} = \frac{1}{\lambda_i}. \tag{68}$$

Thus, (63) , (64) and (65) can be rewritten as

$$I_{1,1} = 2\Psi \sum_{i=1}^{M} \frac{A_i}{c^2}, \tag{69}$$

$$I_{1,1+i} = I_{1+i,1} = 2\Psi \frac{2\pi B_i}{c\lambda_i}, \tag{70}$$

$$\begin{aligned} I_{1,1} &= \frac{\partial^2 \ln p(y;\theta)}{\partial R^2} \\ &= \frac{2}{N_0} Re \int_{-\infty}^{\infty} \sum_{i=1}^{M} a_i s_i^*(t-g(R)) g'(R) e^{j2\pi h(v_{di})t} \sum_{i=1}^{M} a_i s_i(t-g(R)) g'(R) e^{-j2\pi h(v_{di})t} dt \\ &= \sum_{i=1}^{M} \frac{2}{N_0} g'(R)^2 \int_{-\infty}^{\infty} a_i^2 |s_i(t-g(R))|^2 dt \\ &= \sum_{i=1}^{M} 2\Psi g'(R)^2 L_i, \end{aligned} \tag{63}$$

$$\begin{aligned} I_{1,1+i} &= I_{1+i,1} \\ &= \frac{\partial^2 \ln p(y;\theta)}{\partial R \partial v_{di}} \\ &= \frac{4\pi}{N_0} Im \int_{-\infty}^{\infty} a_i t s_i(t-g(R)) e^{-j2\pi h(v_{di})t} h'(v_{di}) \sum_{i=1}^{M} a_i n(t) s_i^*(t-g(R)) g'(R) e^{-j2\pi h(v_{di})t} \\ &= \frac{4\pi a_i^2}{N_O} Im \int_{-\infty}^{\infty} t s_i(t-g(R)) s_i^*(t-g(R)) h'(v_{di}) g'(R) dt \\ &= 4\pi \Psi h'(v_{di}) g'(R) (Q_i + g(R) H_i), \end{aligned} \tag{64}$$

$$\begin{aligned} I_{1+i,1+i} &= \frac{\partial^2 \ln p(y;\theta)}{\partial {v_{di}}^2} \\ &= \frac{8\pi^2}{N_0} Im \int_{-\infty}^{\infty} \int_{-\infty}^{\infty} a_i t s_i^*(t-g(R)) e^{j2\pi h(v_{di})t} h'(v_{di}) a_i t s_i(t-g(R)) e^{-j2\pi h(v_{di})t} h'(v_{di}) dt \\ &= \frac{8(\pi h'(v_{di}))^2}{N_0} \int_{-\infty}^{\infty} a_i^2 t^2 |s_i(t-g(R))|^2 dt \\ &= 8(\pi h'(v_{di}))^2 \Psi (G_i + 2P_I g(R) - g(R)^2 E_i), \end{aligned} \tag{65}$$

$$I_{1+i,1+i} = 2\Psi \frac{4\pi^2 C_i}{\lambda_i^2}. \tag{71}$$

Then, the FIM can be expressed as

$$I(\theta) = 2\Psi \begin{bmatrix} \sum_{i=1}^{M} \frac{A_i}{c^2} & \frac{2\pi B_1}{c\lambda_1} & \frac{2\pi B_2}{c\lambda_2} & \cdots & \frac{2\pi B_M}{c\lambda_M} \\ \frac{2\pi B_1}{c\lambda_1} & \frac{4\pi^2 C_1}{\lambda_1^2} & & & \\ \frac{2\pi B_2}{c\lambda_2} & & \frac{4\pi^2 C_2}{\lambda_2^2} & & \\ \vdots & & & \ddots & \\ \frac{2\pi B_M}{c\lambda_M} & & & & \frac{4\pi^2 C_M}{\lambda_M^2} \end{bmatrix}. \tag{72}$$

By calculating the inverse matrix of $I(\theta)$, we can obtain $\mathrm{V}(\hat{R})_{\mathrm{CRLB}}$ and $\mathrm{V}(\hat{v}_{di})_{\mathrm{CRLB}}$, their mathematical presentations are shown in (73) and (74) on the next page.

REFERENCES

[1] D. K. Sah, M. Poongodi, P. K. Donta, M. Hamdi, K. Cengiz, M. M. Kamruzzaman and H. T. Rauf, "Secured wireless energy transfer for the internet of everything in ambient intelligent environments," *IEEE Internet Things Mag.*, vol. 5, no. 1, pp. 62-66, Mar. 2022.

[2] M. Liu, Z. Zhang, Y. Chen, J. Ge, N. Zhao. "Adversarial attack and defense on deep learning for air transportation communication jamming," *IEEE Trans. Intell. Transp. Syst.*, vol. 25, no. 1, pp. 973-986, Jan. 2024.

[3] X. Li, J. Zhang, C. Han, W. Hao, M. Zeng, Z. Zhu and H. Wang, "Reliability and security of CR-STAR-RIS-NOMA assisted IoT networks," *IEEE Internet Things J.*, early access, doi: 10.1109/JIOT.2023.3340371.

[4] L. Wan, X. Kong, and F. Xia, "Joint range-doppler-angle estimation for intelligent tracking of moving aerial targets," *IEEE Internet Things J.*, vol. 5, no. 3, pp. 1625-1636, Jun. 2018.

[5] X. Li, J. Jiang, H. Wang, C. Han, G. Chen, J. Du, C. Hu and S. Mumtaz, "Physical layer security for wireless-Powered ambient backscatter cooperative communication networks," *IEEE Trans. Cognit. Commun. Networking*, vol. 9, no. 4, pp. 927-939, Aug. 2023.

[6] H. Zhang, M. Liu, Yu. Chen, N. Zhao. "Attacking modulation recognition with adversarial federated learning in cognitive radio-enabled IoT," *IEEE Internet Things J.*, early access, DOI: 10.1109/JIOT.2023.3327953.

[7] J. Wang, J. Chuang, S. Berweger, C. Gentile and N. Golmie, "Towards opportunistic radar sensing using millimeter-wave Wi-Fi," *IEEE Internet Things J*, early access, doi: 10.1109/JIOT.2023.3301006.

[8] F. Colone, D. Langellotti and P. Lombardo, "DVB-T signal ambiguity function control for passive radars," *IEEE Trans. Aerosp. Electron. Syst.*, vol. 50, no. 1, pp. 329-347, Jan. 2014.

[9] H. Ma, M. Antoniou, A. G. Stove, J. Winkel and M. Cherniakov, "Maritime moving target localization using passive GNSS-based multistatic radar," *IEEE Trans. Geosci. Remote Sens.*, vol. 56, no. 8, pp. 4808-4819, Aug. 2018.

[10] X. Qu, L. Xie and W. Tan, "Iterative constrained weighted least squares source localization using TDOA and FDOA measurements," *IEEE Trans. Signal Process.*, vol. 65, no. 15, pp. 3990-4003, Aug. 2017.

[11] G. Wang, S. Cai, Y. Li and N. Ansari, "A bias-reduced nonlinear WLS method for TDOA/FDOA-based source localization," *IEEE Trans. Veh. Technol.*, vol. 65, no.10, pp. 8603-8615, Oct. 2016.

[12] X. Liu, J. Jiang, and Z. Zhang, "Cooperative passive location of multi-UAVs based on TDOA-DOA fusion algorithm," in *Proc. 6th Int. Symp. Auton. Syst.*, Nanjing, China, Jun. 2023, pp. 1-6.

[13] X. Hui, Y. Ma and E. C. Kan, "Code division multiple access in centimeter accuracy harmonic RFID locating system," *IEEE J. Radio Freq. Identif. (RFID)*, vol. 1, no. 1, pp. 51-58, Mar. 2017.

[14] M. S. Alam, S. Alsharif, and N. Haq, "Efficient CDMA wireless position location system using TDOA method," *Int. J. Commun. Syst.*, vol. 24, no. 9, pp. 1230-1242, Sept. 2011.

[15] Z. Liu, Y. Zhang, X. Zhang, Y. Cheng, "Research and simulation of single star positioning algorithm based on low earth orbit satellite," in *China Satellite Navigation Conference (CSNC) 2018 Proceedings*, pp. 1-5, 2018.

[16] Y. Xue, X. Li, L. Xu, and Y. Ren, "Research on position differential

$$\begin{aligned}\mathrm{V}(\hat{R})_{\mathrm{CRLB}} &= \frac{c^2}{2\Psi}\frac{\prod_{j=1}^{M} C_j}{\sum_{i=1}^{M} A_i \prod_{j=1}^{M} C_j - \sum_{i=1}^{M} B_i^2 \prod_{j=1(j\neq i)}^{M} C_i} \\ &= \frac{c^2}{2\Psi}\frac{\prod_{j=1}^{M} C_j}{\sum_{i=1}^{M} (A_i C_i - B_i^2) \prod_{j=1(j\neq i)}^{M} C_j} \\ &= \frac{c^2}{2\Psi}\frac{1}{\sum_{i=1}^{M} \frac{A_i C_i - B_i^2}{C_i}},\end{aligned} \tag{73}$$

$$\begin{aligned}\mathrm{V}(\hat{v_{di}})_{\mathrm{CRLB}} &= \frac{c^2}{2\Psi}\frac{\sum_{m=1}^{M} A_m \prod_{n=1(n\neq i)}^{M} C_n - \sum_{m=1(m\neq i)}^{M} B_m^2 \prod_{n=1(n\neq m, n\neq i)}^{M} C_n}{\sum_{m=1}^{M} A_m \prod_{n=1}^{M} C_n - \prod_{n=1}^{M} B_m^2 \prod_{n=1(m\neq n)}^{M} C_n} \\ &= \frac{c^2}{2\Psi}\frac{A_i \prod_{n=1(n\neq i)}^{M} C_n + \sum_{m=1(m\neq i)}^{M} (A_m C_m - B_m^2) \prod_{n=1(n\neq m, n\neq i)}^{M} C_n}{\sum_{m=1}^{M} (A_m C_m - B_m^2) \prod_{n=1(n\neq m)}^{M} C_n} \\ &= \frac{c^2}{2\Psi}\frac{A_i + \sum_{m=1(m\neq i)}^{M} \frac{A_m C_m - B_m^2}{C_m}}{C_i \sum_{m=1}^{M} \frac{A_m C_m - B_m^2}{C_m}}.\end{aligned} \tag{74}$$

method of dual-satellites TDOA and FDOA in passive location system," in *IEEE Int. Freq. Control Symp., IFCS, Proc.*, May. 2012, pp. 1-5.

[17] S. Wu and J. Luo, "Influence of position error on TDOA and FDOA measuring of dual-satellite passive location system," in *Proc. IEEE Int. Symp. Microw., Antenna, Propag. EMC Technol. Wirel. Commun.*, Beijing, China, Oct. 2009, pp. 293-296.

[18] K. Shamaei and Z. M. Kassas, "A joint TOA and DOA acquisition and tracking approach for positioning with LTE Signals," *IEEE Trans. Signal Process.*, vol. 69, pp. 2689-2705, Jun. 2021.

[19] S. Gogineni, M. Rangaswamy, B. D. Rigling, and A. Nehorai, "Cramer-Rao bounds for UMTS-based passive multistatic radar," *IEEE Trans. Signal Process.*, vol. 62, no. 1, pp. 95-106, Jan. 2014.

[20] P. Samczyński *et al*., "5G Network-based passive radar ," *IEEE Trans. Geosci. Remote Sens.*, vol. 60, pp. 1-9, 2022.

[21] J. L. Sendall and F. D. V. Maasdorp, "Detection state refinement in FM multistatic passive radar," in *IEEE Radar Conf.*, Seattle, WA, USA, May. 2017, pp. 0717-0721.

[22] C. Shi, F. Wang, and J. Zhou, "Cramer-Rao bound analysis for joint target location and velocity estimation in frequency modulation based passive radar networks," *IET Signal Process.*, vol. 10, no. 7, pp. 780-790, Sept. 2016.

[23] T. Tirer and A. J. Weiss, "Performance analysis of a high-resolution direct position determination method," *IEEE Trans. Signal Process.*, vol. 65, no. 3, pp. 544-554, Feb. 2017.

[24] F. Ahmed, M. H. Conde and P. L. Martínez, "Kalman filter-driven blind source localization for passive 3D ToF imaging," *IEEE Sens. Lett.*, vol. 6, no. 10, pp. 1-4, Oct. 2023.

[25] S. Searle *et al*., "Improvement of a sample clock offset estimation method used in passive radar," *IEEE Trans. Aerosp. Electron. Syst.*, vol. 58, no. 4, pp. 3678-3685, Aug. 2022.

[26] B. Xu, J. Yi, X. Wan and F. Cheng, "Target tracking algorithm based on generalized regression neural network for passive bistatic radar," *IEEE Sens. J.*, vol. 23, no. 10, pp. 10776-10789, May. 2023.

[27] Z. Yu and Y. Fu, "A passive location method based on virtual time reversal of cross antenna sensor array and tikhonov regularized TLS," *IEEE Sens. J.*, vol. 21, no. 19, pp. 21931-21940, Oct. 2021.

[28] J. He, T. Shu, V. Dakulagi, and L. Li, "Simultaneous interference localization and array calibration for robust adaptive beamforming with partly calibrated arrays," *IEEE Trans. Aerosp. Electron. Syst.*, vol. 57, no. 5, pp. 2850-2863, 2021.

[29] W. Miao, C. Luo, G. Min, Y. Mi and Z. Yu, "Location-based robust beamforming design for cellular-enabled UAV communications," *IEEE Internet Things J.*, vol. 8, no. 12, pp. 9934-9944, June. 2021.

[30] J. L. Gomez-Tornero, A. J. Martinez-Ros and R. Verdu-Monedero, "FFT synthesis of radiation patterns with wide nulls using tapered leaky-wave antennas," *IEEE Antennas Wirel. Propag. Lett.*, vol. 9, pp. 518-521, 2010.

[31] Z. Zhang and M. Luo, "New integral transforms for generalizing the wigner distribution and ambiguity function," *IEEE Signal Process Lett.*, vol. 22, no. 4, pp. 460-464, Apr. 2015.

[32] T. Zhao and T. Huang, "Cramer-Rao lower bounds for the joint delay-doppler estimation of an extended target," *IEEE Trans. Signal Process.*, vol. 64, no. 6, pp. 1562-1573, Mar. 2016.

[33] D. Fontanelli, F. Shamsfakhr and L. Palopoli, "Cramér-Rao lower bound attainment in range-Only positioning using geometry: The G-WLS," *IEEE Trans. Instrum. Meas.*, vol. 70, pp. 1-14, 2021.

[34] M. Liu, B. Li, Y. Chen, Z. Yang, N. Zhao, P. Liu and F. Gong, "Location parameter estimation of moving aerial target in space-air-ground integrated networks-based IoV," *IEEE Internet Things J.*, vol. 9, no. 8, pp. 5696-5707, Apr. 2022.